SAND 96-2394C

CONF-9706110--1

Analytic Fit of Deviation Caused by Atmospheric Refraction of Starlight as a Function of Space-Based Sensor Position

For Poster Session at the 1997 Infrared Information Symposia
Specialty Group on Targets, Backgrounds and Discrimination
Space Surveillance

Johns Hopkins University Applied Physics Laboratory
Laurel, Maryland 20707

June 4-5, 1997

Charles N. Vittitoe and Ron L. Schmidt
Optics and Exploratory Technologies
Sandia National Laboratories
P. O. Box 5800
Albuquerque, New Mexico 87185-0967

MASTER

DISTRIBUTION OF THIS DOCUMENT IS UNLIMIT

DISCLAIMER

Portions of this document may be illegible in electronic image products. Images are produced from the best available original document.

Analytic Fit of Deviation Caused by Atmospheric Refraction of Starlight as a Function of Space-Based Sensor Position*

June 1997

Charles N. Vittitoe and Ron L. Schmidt
Optics and Exploratory Technologies Department
Sandia National Laboratories
P. O. Box 5800
Albuquerque, New Mexico 87185-0967

ABSTRACT

A simple prescription describes how space-borne sensors with fields of view less than one degree can be properly aimed at starlight that passes near the Earth's surface and is therefore refracted by the Earth's atmosphere. Atmospheric refraction effects cause deviations up to about one degree that distort the light path and can cause the target to be missed. Deviations are contrasted with those experienced for a target on the Earth. Such refractive corrections have long been available for Earth-based sensors looking through the atmosphere. The corrections have not been available for sensors in space. The prescription is illustrated by example.

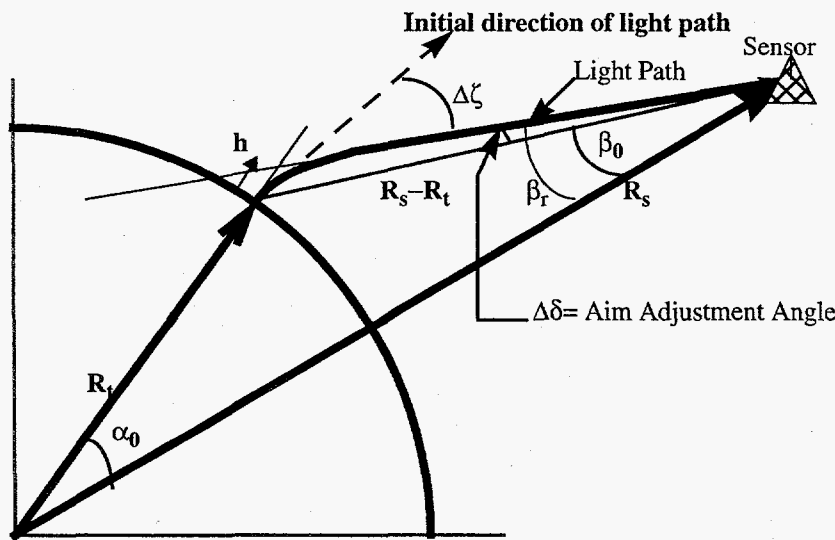## 1.0 INTRODUCTION AND REFRACTION REVIEW FOR TARGETS ON THE EARTH

Figure 1. Light path geometry

Consider a space-borne sensor with a small field of view tasked to observe starlight which passes near the Earth's surface. Refractive effects within the Earth's atmosphere cause the rays to bend; care is required to aim in a way that retains the image. Similar perturbations occur during satellite observation of targets on the Earth itself.

The geometry for a target on the Earth is illustrated in Figure 1. The plane of refraction (defined by the Earth's center (origin), the sensor location, $\vec{R}_s$, and the target location, $\vec{R}_t$, (on the Earth's surface) contains the light path that is distorted by atmospheric refraction. For observers viewing stars from the Earth,

---

such refraction is often expressed as changes in the apparent zenith angle of the stars.* These changes are represented by $\Delta\zeta$ in Figure 1 and have been approximated using results from ray tracing in standard atmospheres as described by standard references (HGSE and IR Handbook, V2).

Using the notation introduced in Figure 1, the Law of Sines gives $R_t/(\sin\beta_0) = |\vec{R}_s - \vec{R}_t|/(\sin\alpha_0)$. The ray received at the sensor appears to have come from an altitude h along $\hat{R}_t$. In Figure 1, h is the distance from the target location up to the intersection between the extended $\vec{R}_t$ and a ray parallel to the apparent light path received at the sensor. Again the Law of Sines gives $(R_t + h)/(\sin\beta_r) = |\vec{R}_s - \vec{R}_t - \vec{h}|/(\sin\alpha_0)$. The change in incident angle at the sensor is the difference between the value of β with refraction included (β_r) and β_0; that is the deviation in aim angle, $\Delta\delta = \beta_r - \beta_0$. Eliminating α_0 from the two equations and expanding for small $\Delta\delta$ yields

$$\frac{R_t + h}{R_t} = \frac{|\vec{R}_s - \vec{R}_t - \vec{h}|}{|\vec{R}_s - \vec{R}_t|} = 1 + \frac{\Delta\delta}{\tan\beta_0}.$$

An upper bound to $\tan\beta_0$ is $R_t/|\vec{R}_s - \vec{R}_t|$. Using the approximations $R_t = 6371 km$ and h<40 km (as discussed later) and neglecting the higher order terms gives $\Delta\delta < h/|\vec{R}_s - \vec{R}_t| = 40 km/|\vec{R}_s - \vec{R}_t|$. For sensors at altitudes less than 40 km this inequality is not very restrictive and β_0 is much smaller than the upper bound chosen earlier. A better bound on $\Delta\delta$ is available from alterations in apparent zenith angle. Low-altitude sensors have alterations in zenith angle $\leq 1.5°$ (HGSE). On the other hand, sensors at high altitudes, such as GPS (Global Positioning System) altitudes ($h \approx 20200 km$) are restricted by the inequality to $\Delta\delta < 40/20200 = 2 mrad = 0.11°$. A still smaller upper bound is available for a particular case by taking a realistic β_0 rather than the upper bound chosen here.

In summary for targets on the Earth's surface, sensors at altitudes around 40 km see apparent directions altered up to about $1.5°$ by refraction effects. Sensors at high altitudes, $\geq 20000 km$ see apparent directions altered by less than $0.15°$. Deviations experienced by high-altitude sensors are small for targets on the Earth. In contrast, as seen in the next section, for celestial targets the deviations can be large, even for high-altitude sensors.

2.0 CELESTIAL TARGETS

Sensors at high altitudes may be tasked to observe stars rather than Earth-bound targets. In such cases, refraction effects can significantly alter the view. Sensors with small fields of view can miss the star completely. A recent report develops formulae appropriate for proper aiming from high-altitude sensors toward the relatively few stars that are near the Earth's limb at a given time.† These formulae correct for refraction effects based on ray tracing in the U. S. Standard Atmosphere, 1976.

The ray path received at the sensor is illustrated in Figure 2. The distance of closest approach to the Earth is indicated as H_t. HGSE refers to H_t as the refracted tangent height. H_t' is the apparent tangent height, and $\Delta\delta$ is the light-path deviation caused by refraction. $\hat{E}$ is a unit vector directed toward the source. The θ_{inc} is given by $a\cos(-\vec{R}_s \bullet \hat{E}/R_s)$.‡ The geometry shown in Figure 2 gives a relation between the space-based sensor position, $\vec{R}_s$, and the other parameters. With H_t' understood as a function of the deviation, $\Delta\delta$,

$$R_s \sin(\Delta\delta + \theta_{inc}) = R_e + H_t'.$$

---

* *Handbook of Geophysics and the Space Environment*, edited by A. S. Jursa of the Air Force Geophysics Laboratory, 1985 (referred to here as HGSE) and *The Infrared & Electro-Optical Systems Handbook*, volume 2, "Atmospheric Propagation of Radiation," edited by F. G. Smith, SPIE Optical Engineering Press, Bellingham, Washington, 1993 (referred to as IR Handbook, V2).

† C. N. Vittitoe and R. L. Schmidt, *Refractive Aiming Corrections for Satellite Observation of Stars*, Sandia National Laboratories Report Number SAND97-0415, March 1997 (Referred to as VS0415). Report is available from http://infoserve.library.sandia.gov/sand971.html with the aid of an Adobe Acrobat Reader to view Portable Document Format.

‡ The symbol $\bullet$ implies the scalar product of vectors; a caret ($\hat{}$) over a symbol implies that the variable is a unit vector.
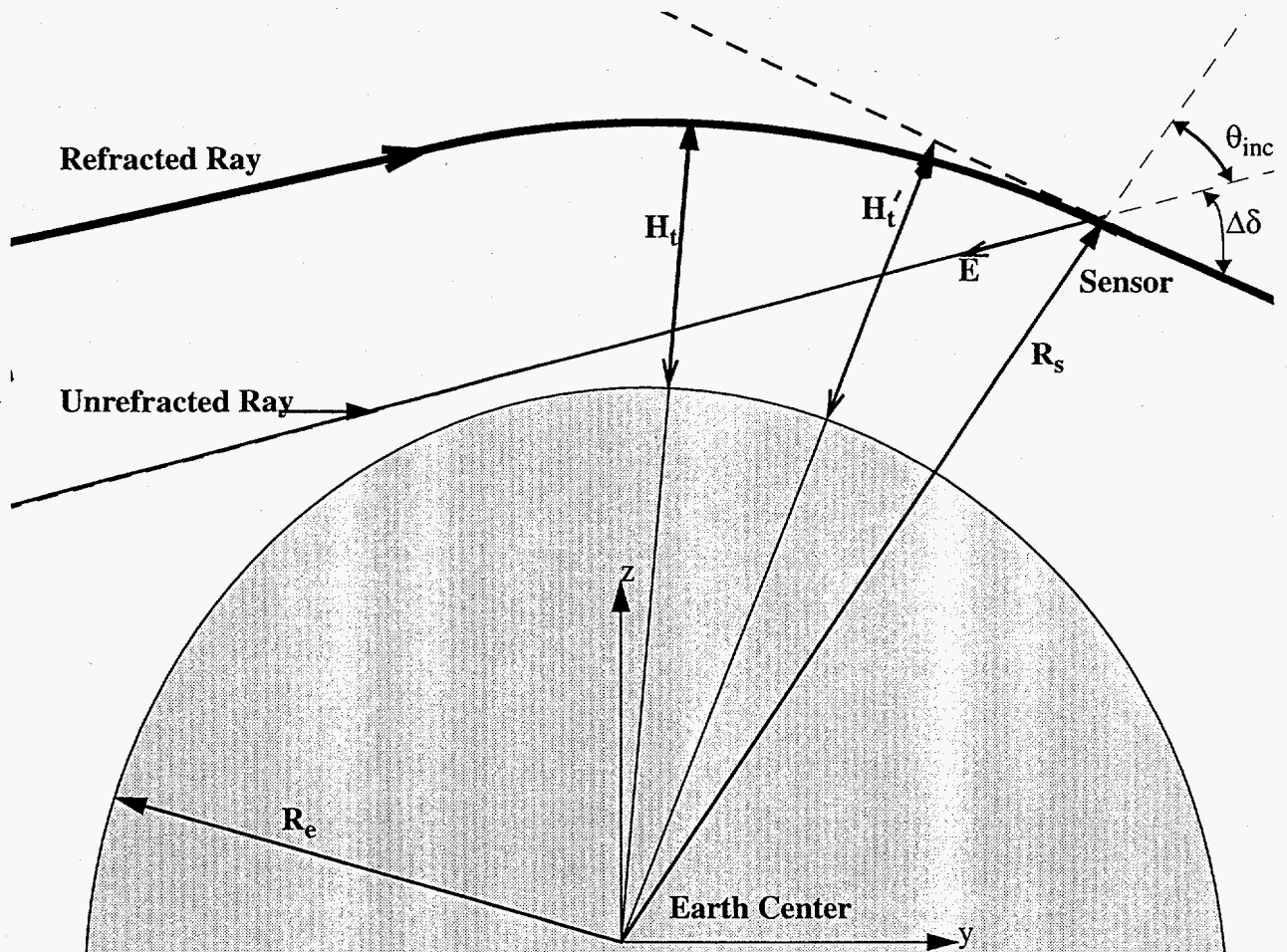
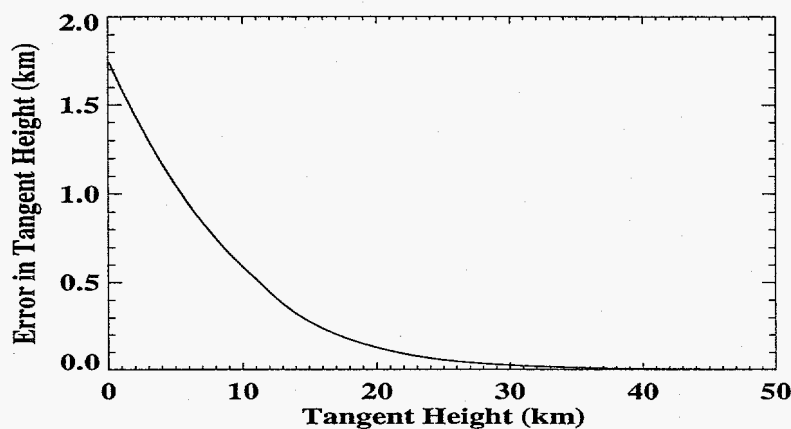**Figure 2. Illustration of the plane of refraction.**

Figure 3. Error in Earth-tangent height vs refracted tangent height predicted for the U. S. Standard Atmosphere, 1976.

Figure 3 illustrates the error in apparent height $(H_t' - H_t)$ of the Earth-tangent ray as a function of the ray's minimum height, H_t. A similar result has been published in HGSE, pages 18 - 67. As pointed out by VS0415, the equation for the curve in Figure 3 is $H_t' - H_t = [n(H_t) - 1] \cdot [H_t + R_e]$, where $n(H_t)$ is the atmospheric index of refraction at altitude H_t. The larger the index of refraction at altitude H_t, the greater the error in apparent height. Because of the $n(H_t)$ dependence in Figure 3, there is a subtle discontinuity in slope that occurs near $H_t = 11$ km, as the stable tropopause altitude is attained. At $H_t = 0$, the ray intercepts the Earth and no refracted ray is detected.

3.0 ANALYTIC FIT

With deviations in degrees and apparent altitudes in km, analytic fits to deviations as a function of H_t' are

$$\Delta\delta = 1.0864 \exp\left[\frac{-(H_t' - 1.8403)}{8.9}\right] \text{ for } H_t' < 10.59 km$$

$$\Delta\delta = 0.3261 \exp\left[\frac{-(H_t' - 12.4455)}{6.1}\right] \text{ for } H_t' > 12.45 km$$

$$\Delta\delta = 0.4067 \exp\left[\frac{-(H_t' - 10.5905)}{14.0}\right] \text{ for } 10.59 \le H_t' \le 12.45 km.$$

These variations are illustrated in Figure 4 (+ signs) along with the ray-tracing results (solid curve) from VS0415. Note the scale heights. Near the tropopause, the scale height is largest at 14 km. At lower altitudes, the scale height is 8.9 km, while at higher altitudes the scale height is 6.1 km.
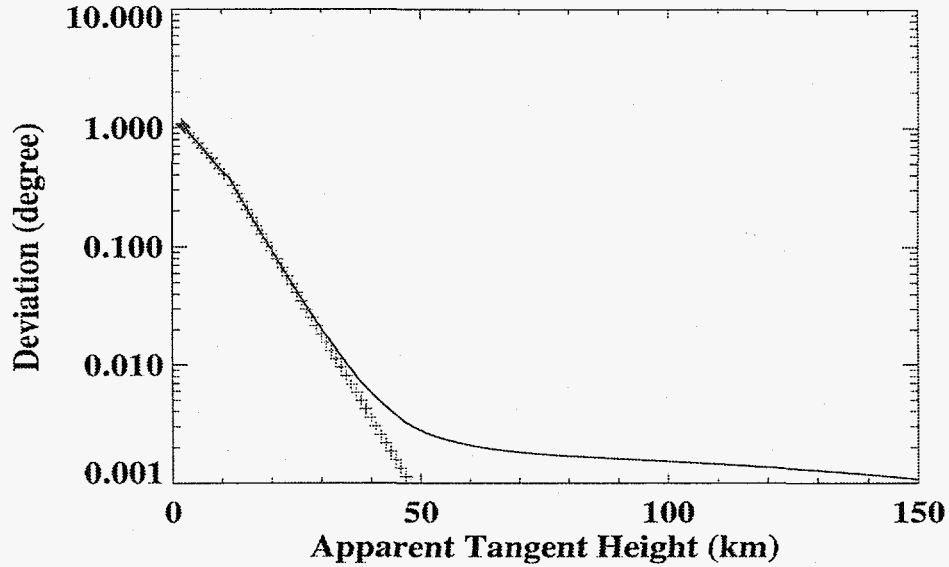

Figure 4. Comparison of analytic fit to $\Delta\delta$ data as a function of H_t'.

Application of newton's method to solve $R_s \sin(\Delta\delta + \theta_{inc}) = R_e + H_t'$ for $\Delta\delta$ is more convenient using the apparent height as a function of deviation rather than the deviation as a function of apparent height described above. Solving for the apparent height gives

$$H_t' = 1.8403 + 8.9 \ln\frac{1.0864}{\Delta\delta} \text{ for small } H_t' \text{ and } \Delta\delta > 0.4067 \text{ degree.}$$

$$H_t' = 10.5905 + 14.0 \ln\frac{0.4067}{\Delta\delta} \text{ for intermediate } H_t' \text{ and } 0.3261 < \Delta\delta < 0.4067 \text{ degree.}$$

$$H_t' = 12.4455 + 6.1 \ln\frac{0.3261}{\Delta\delta} \text{ for large } H_t' \text{ and } 0.0030 < \Delta\delta < 0.3261 \text{ degree.}$$

Other values of deviation are assigned an artificial value of $H_t' = 200 km$ that corresponds to $\Delta\delta = 0$.

Differences between the analytic fit and the ray-trace data in Figure 4 are less than 0.003 degree (52μradian, 10.8″). This error can be reduced by using a more involved fitting function. Because of the dynamic nature of the atmosphere, a detailed fit of deviation as a function of the apparent tangent height with errors less than 0.003 degree is not justified. $H_t' \ge 35$ km gives $\Delta\delta \le 0.0081°$, suggesting that significant refraction only occurs at altitudes less than 35 km.

Consider this brief review of the aiming-correction implementation that applies for starlight where true right ascension and declination are known. θ_{inc} is evaluated from $\mathrm{acos}(-\vec{R}_s \bullet \hat{E}/R_s)$. Deviation is found by applying newton's method to solve $R_s \sin(\Delta\delta + \theta_{inc}) = R_e + H_r'(\Delta\delta)$ for $\Delta\delta$. The deviation is added to the latitude in the refraction plane. Coordinate transformations and rotations back to ECI* coordinates give the apparent right ascension and declination desired for aiming the sensor. VS0415 provides details describing the required coordinate changes.

4.0 AIMING-CORRECTION EXAMPLES FOR VIEWING ALPHA CENTAURI FROM SPACE

To illustrate refractive effects, examine the aiming corrections required to view $\alpha^1 Cen$ from a sensor in space. The examples chosen position the sensor in a Keplerian orbit with the following initial conditions:

Right ascension of ascending node: $\Omega = 40°$, True anomaly: $\nu = 0°$,

Inclination angle: $\iota = 90°$, Argument of perigee: $\omega = -80°$,
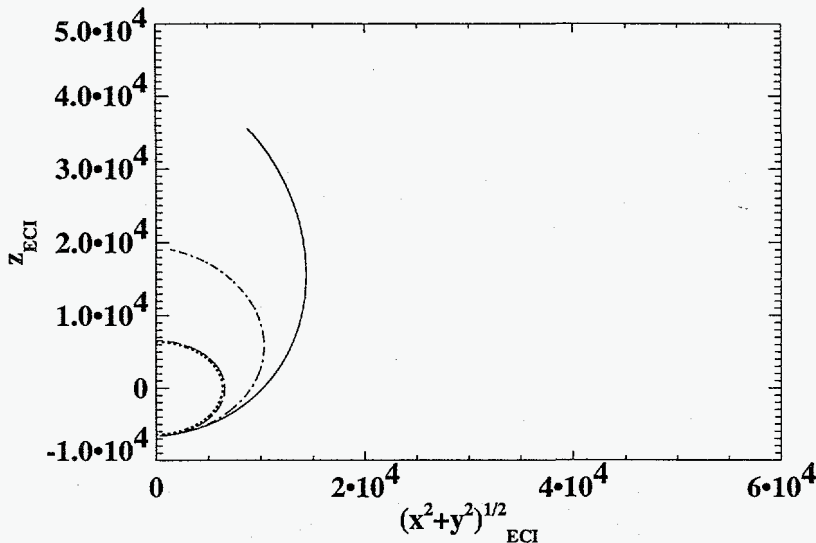
Altitude = 200 km.

Figure 5. Sample orbits for refraction tests.

Orbit eccentricities are taken as $\varepsilon = 0$, 0.50, and 0.75 for three examples. Each orbit starts at perigee in the southern hemisphere. The orbit's Ω coupled with the inclination places the orbit nearly in a plane containing $\alpha^1 Cen$. Thus, any alterations in apparent right ascension are small. Figure 5 displays a portion of the three orbits: a dashed line for $\varepsilon = 0$, a dash-dot line for $\varepsilon = 0.5$, and a solid line for $\varepsilon = 0.75$. Distances are given in km. $\alpha^1 Cen$ is nearly in the sensor-orbit plane (see Figure 5) with its declination near $-60°$. The $\varepsilon = 0.5$ and 0.75 cases are only propagated to within bounds illustrated in Figure 5; the $\varepsilon = 0$ orbit is propagated just beyond a full revolution.

As the sensor traverses its orbit, alterations occur in the apparent declination angle. Figures 6, 7, and 8 show the effect. Examination of the $\varepsilon = 0$ case in Figure 6 shows that refractive effects disturb the light paths for only a small fraction of the orbit. When the effects occur, they last for about 60 seconds and can cause deviations slightly larger than $1°$. With other orbit choices, the changes in right ascension can also be as large as about $1°$ and can last a few times as long.

Figure 6 shows that at about 1000 s from perigee, the line of sight to $\alpha^1 Cen$ is beginning to skim the atmosphere. As viewed from the sensor, the star's declination appears more negative. As the line of sight comes closer to the Earth, the apparent declination continues to decrease until it reaches a minimum. The following abrupt increase (back to a change of zero) represents the line of sight being cut off by the Earth's surface. Later in the orbit, the line of sight becomes nearly tangent to the Earth's surface in the northern hemisphere and the apparent declination jumps to its maximum value and subsequently decreases at a slower rate as seen near 3150 s from perigee in Figure 6.

---

* ECI (Earth-centered inertial) coordinates are at times called celestial coordinates or geocentric inertial (GCI) coordinates. Because of precession of the equinoxes and rotation of the sun about the center of mass of the Milky Way galaxy, they do not form an inertial system.
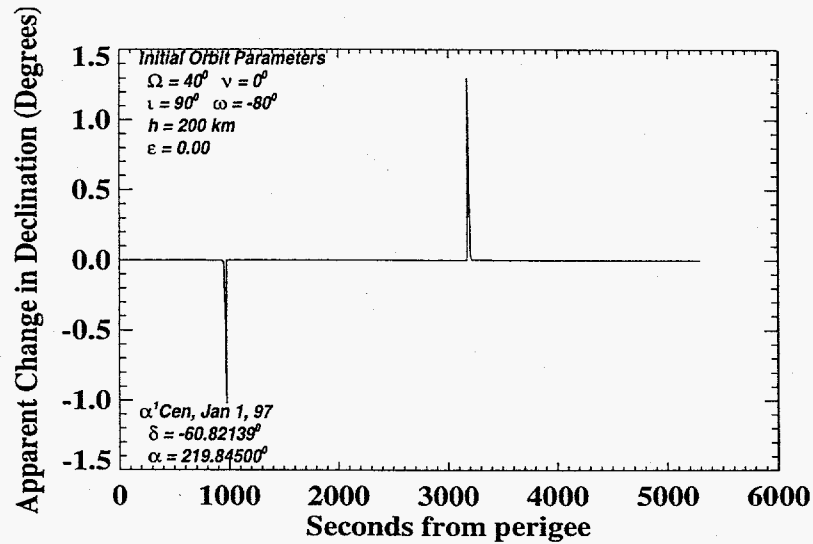
Figure 6. Variation in declination angle with time past perigee for the ε = 0 orbit.

Results for the ε = 0.5 are illustrated in Figure 7. More time is required to reach sensor positions where refraction effects occur, but effects are similar to ε = 0 with respect to polarity, magnitude, and duration. The apparent change at about 5400 s from perigee that reaches near 0.6° is caused by orbit positions being calculated at 1-s intervals. Finer time resolution would include a ray that just skims the Earth's surface, and deviations would reach about 1.3° as seen in Figure 6.
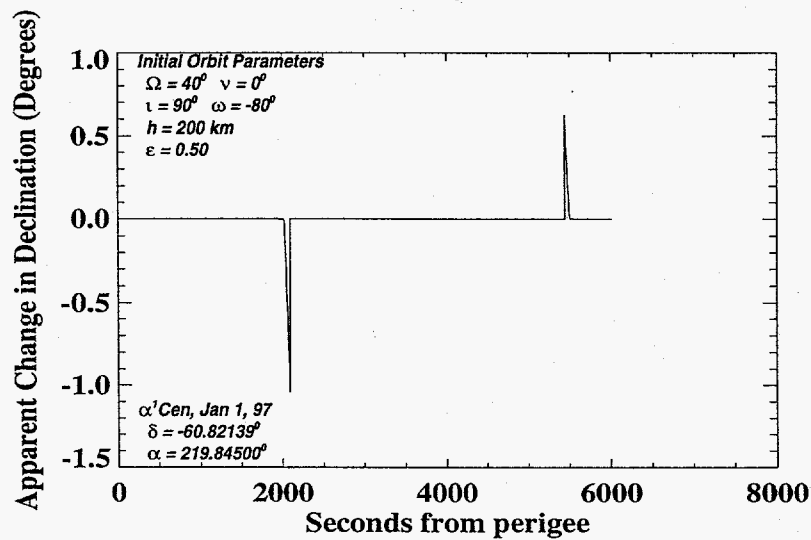

Figure 7. Variation in declination angle with time past perigee for the ε = 0.5 orbit.

Data for the more eccentric orbit, $\varepsilon = 0.75$ in Figure 8, illustrates refractive effects lasting about 170 s. Even longer times can be encountered with special selection of orbit parameters. For the $\varepsilon = 0.75$ case described in Figure 5 and presented in Figure 8, refraction effects start when the sensor nears $\sqrt{x^2 + y^2} = 14000$km, and $z = 13000$km, and begin again when $\sqrt{x^2 + y^2} = 10700$km and $z = 32000$km.
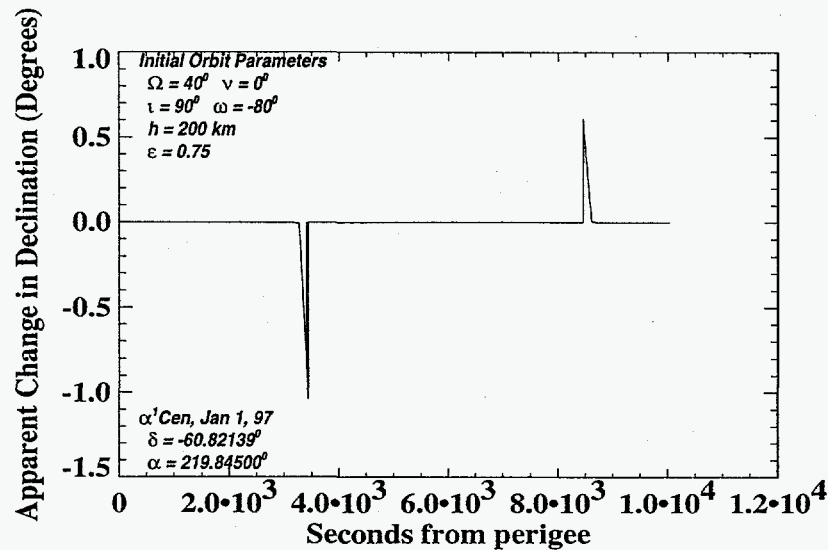

Figure 8. Variation in declination angle with time past perigee for the $\varepsilon = 0.75$ orbit.

5.0 DISCUSSION OF RESULTS

Refractive aiming corrections have been defined to improve satellite observation of stars for geometries where the line of sight is nearly tangent to the Earth's surface. Required inputs are satellite position and direction to the target star. Predictions are based on ray tracing in the U. S. Standard Atmosphere, 1976. Celestial targets can require considerably larger aiming alterations than targets on the Earth.

Predictions of expected refractive effects were presented for three example satellite orbits. Refraction can alter stellar right ascensions and declinations by more than one degree. The orbits considered give refractive-effect durations typically from ~1 minute to ~3 minutes. These time intervals suggest that satellites in the chosen orbits have lines of sight to the target star that effectively pass through the ~35 km height of the atmosphere in a few minutes.